Combustion and Flame 157 (2010) 982–994

Contents lists available at ScienceDirect

Combustion and Flame

journal homepage: www.elsevier.com/locate/combustflame

Composition PDF/photon Monte Carlo modeling of moderately sooting turbulent jet flames

R.S. Mehta *, D.C. Haworth, M.F. Modest [1]

Department of Mechanical and Nuclear Engineering, The Pennsylvania State University, University Park, PA 16802, United States

ARTICLE INFO

Article history:
Received 7 August 2009
Received in revised form 17 November 2009
Accepted 17 November 2009
Available online 16 December 2009

Keywords:
Soot modeling
Radiation modeling
Turbulent flames
Luminous flames
PDF methods
Monte Carlo

ABSTRACT

A comprehensive model for luminous turbulent flames is presented. The model features detailed chemistry, radiation and soot models and state-of-the-art closures for turbulence–chemistry interactions and turbulence–radiation interactions. A transported probability density function (PDF) method is used to capture the effects of turbulent fluctuations in composition and temperature. The PDF method is extended to include soot formation. Spectral gas and soot radiation is modeled using a (particle-based) photon Monte Carlo method coupled with the PDF method, thereby capturing both emission and absorption turbulence–radiation interactions. An important element of this work is that the gas-phase chemistry and soot models that have been thoroughly validated across a wide range of laminar flames are used in turbulent flame simulations without modification. Six turbulent jet flames are simulated with Reynolds numbers varying from 6700 to 15,000, two fuel types (pure ethylene, 90% methane–10% ethylene blend) and different oxygen concentrations in the oxidizer stream (from 21% O_2 to 55% O_2). All simulations are carried out with a single set of physical and numerical parameters (model constants). Uniformly good agreement between measured and computed mean temperatures, mean soot volume fractions and (where available) radiative fluxes is found across all flames. This demonstrates that with the combination of a systematic approach and state-of-the-art physical models and numerical algorithms, it is possible to simulate a broad range of luminous turbulent flames with a single model.

1. Introduction

Developments over the last few decades in turbulence modeling, combustion modeling and computing resources have resulted in detailed models for various phenomena involved in turbulent combustion. In order to successfully model turbulent reacting flows, the following are needed: (i) a turbulence model to predict the turbulent flow-field to a reasonable degree of accuracy; (ii) a detailed chemistry model, including soot formation; (iii) a model of physical properties of the reacting gas mixture including density, enthalpies, specific heats and transport coefficients; and (iv) a radiation model, including those for the radiative properties of the medium (participating gases and soot) and a radiative transfer equation (RTE) solution method. Models to account for turbulence–chemistry interactions (TCI) and turbulence–radiation interactions (TRI) are also needed.

Soot formation is a highly complex process involving a large number of both homogeneous and heterogeneous reactions and other physical processes such as coagulation and agglomeration. While soot formation and oxidation can be predicted with reasonable success in laminar flames using detailed models [1,2], modeling soot dynamics in turbulent flames poses additional challenges. Linking of soot kinetics to turbulence and gas-phase chemistry is crucial to the success of soot modeling in turbulent combustion. Moss and coworkers [3,4] have used a flamelet model for gas-phase TCI, followed by both a presumed probability density function (PDF) and a transported PDF closure for the soot subprocesses. Kollmann and Kennedy [5] applied a mixture-fraction-based combustion model combined with a two-variable soot model (soot volume fraction and soot particle number density) to a turbulent ethylene jet flame. Zimberg et al. [6] used a linear eddy model for TCI. They also considered two different soot models based on a state relationship and explicit transport equations for the soot volume fraction and particle number density. Zamuner and Dupoirieux [7] applied a probabilistic Eulerian–Lagrangian model to include soot formation, and captured effects of turbulent fluctuations on soot yield using a PDF method. However, soot volume fractions were calculated in the turbulent flame based on precomputed velocity fields. Balthasar et al. [8] applied a transported PDF approach to solve for the joint compostion PDF of the scalars, enthalpy and soot scalars in a partially stirred

* Corresponding author. Present address: CFD Research Corporation, Huntsville, AL 35805, United States. Fax: +1 256 726 4806.
E-mail addresses: rsm@cfdrc.com (R.S. Mehta), dch12@psu.edu (D.C. Haworth), mmodest@ucmerced.edu (M.F. Modest).
[1] Present address: Department of Mechanical Engineering, University of California, Merced, CA 95348, United States.

0010-2180/$ - see front matter © 2009 The Combustion Institute. Published by Elsevier Inc. All rights reserved.
doi:10.1016/j.combustflame.2009.11.009

plug-flow reactor; the gas-phase chemistry and soot model were based on work of Frenklach and Wang [9] and the optically thin radiation model was used. Lindstedt and Louloudi [10] used a method of moments for soot formation in a transported PDF formulation and obtained encouraging agreement with experimental profiles for turbulent ethylene–air flames. They used a parabolic time-marching scheme in the solution method. A previously validated soot model [11] was used with a reduced 29-species gas-phase chemistry, and radiation was treated using the optically thin approximation (neglecting reabsorption). Desjardin and Frankel [12] studied soot formation in a turbulent acetylene flame using a two-dimensional LES formulation. They used a S_4-level discrete-ordinates method [13] with a gray gas and soot properties. Recently Chandy et al. [14] used a hybrid LES/filtered mass density function method to simulate a strongly radiating flame. Single-step chemistry mimicking acetylene combustion and a soot model based on state-relationships were used to study effect of turbulence–radiation interactions on the flame structure.

The objectives of this study are: (i) to develop a comprehensive approach for modeling turbulent reacting flows including soot formation; (ii) to extend the transported PDF approach to obtain turbulent closure for soot subprocesses; and (iii) to compare model predictions to experiments for luminous turbulent jet flames with variations in jet Reynolds numbers, fuel composition, and oxygen content in the oxidizer using a single set of model parameters. An important element of this work is that soot models that have been throughly validated across a wide range of laminar flames [2] are used in turbulent flames without modifications.

2. Physical and numerical models

2.1. Governing equations

The principal governing equations for mean quantities are expressed using standard notation as follows [15]:

- Mass

$$\frac{\partial\langle\rho\rangle}{\partial t}+\frac{\partial}{\partial x_i}[\langle\rho\rangle\widetilde{u}_i]=0. \tag{1}$$

- Momentum ($j=1,2,3$)

$$\frac{\partial}{\partial t}[\langle\rho\rangle\widetilde{u}_j]+\frac{\partial}{\partial x_i}[\langle\rho\rangle\widetilde{u}_i\widetilde{u}_j]=-\frac{\partial}{\partial x_i}\left[\langle\rho\rangle\widetilde{u_i''u_j''}\right]+\frac{\partial\langle\tau_{ij}\rangle}{\partial x_i}-\frac{\partial\langle p\rangle}{\partial x_j}+\langle\rho g_j\rangle, \tag{2}$$

where $\langle\rho\rangle\widetilde{u_i''u_j''}$ is the Reynolds-stress tensor.

- Chemical species (for s species, $\alpha=1,2,\ldots,s$)

$$\frac{\partial\langle\rho\rangle\widetilde{Y_\alpha}}{\partial t}+\frac{\partial\langle\rho\rangle\widetilde{Y_\alpha}\widetilde{u}_i}{\partial x_i}=-\frac{\partial\langle\rho\rangle\widetilde{Y_\alpha''u_i''}}{\partial x_i}-\frac{\partial\langle J_i^\alpha\rangle}{\partial x_i}+\langle\rho\rangle\widetilde{S_\alpha}. \tag{3}$$

The terms $\langle\rho\rangle\widetilde{Y_\alpha''u_i''}$ represent transport of the species due to turbulent fluctuations. This term would require modeling in a moment closure, and that generally is done using a gradient transport approximation. The mean reaction rate $\widetilde{S_\alpha}$ also would need modeling because of the highly nonlinear dependence of S_α on the local composition and temperature.

- Absolute enthalpy

$$\frac{\partial\langle\rho\rangle\widetilde{h}}{\partial t}+\frac{\partial\langle\rho\rangle\widetilde{h}\widetilde{u}_i}{\partial x_i}=-\frac{\partial\langle\rho\rangle\widetilde{h''u_i''}}{\partial x_i}-\frac{\partial\left\langle J_i^h\right\rangle}{\partial x_i}+\frac{D\langle p\rangle}{Dt}+\left\langle\tau_{ij}\frac{\partial\widetilde{u}_j}{\partial x_i}\right\rangle+\langle S_{\mathrm{rad}}\rangle, \tag{4}$$

where $\langle\rho\rangle\widetilde{h''u_i''}$ is the turbulent transport of enthalpy, which would require modeling in a moment-based approach. Because S_{rad} (like S_α) is nonlinear in composition and temperature, the mean radiative source term in the energy equation $\langle S_{\mathrm{rad}}\rangle$ would also require modeling.

Additional modeled equations would be needed to provide turbulence scale information. For example, a conventional two-equation k–ε turbulence model has been shown to provide reasonable accuracy for simple jet flames that are considered here. A composition PDF approach is used here, and the species and enthalpy transport equations are solved in a Lagrangian framework. This differs from a conventional moment-based approach.

2.2. Gas-phase chemistry

A systematically reduced 33-species reaction mechanism containing 205 elementary reactions is used to model gas-phase kinetics [16]. This mechanism was found to perform satisfactorily in predicting soot volume fractions in laminar premixed and opposed-flow-diffusion ethylene–air flames across a broad range of conditions [2]. Accuracy of the species concentrations provided by the gas-phase chemistry, particularly species involved in soot-particle nucleation and surface growth/oxidation submodels (e.g., C_2H_2 and OH) is crucial to the accuracy of soot prediction [17]. The skeletal mechanism is based on a detailed model developed by Qin et al. [18] and was an optimized version of detailed reaction mechanisms developed for C_1–C_3 fuels. The optimizations were based on ignition delays for shock-heated fuel/oxygen/argon mixtures with equivalence ratios ranging from 0.5 to 5 and laminar flame speeds in fuel mixtures at 1 atm, with equivalence ratios ranging from 0.5 to 1.2. The 33-species reduced mechanism was developed by Law [16], using Directed Relational Graph (DRG) based reduction. In doing so, PSR and auto-ignition data from detailed mechanisms in pressures ranging from 0.1 to 30 atm, equivalence ratio ranging from 0.7 to 1.3, and initial temperatures of 300 K for PSR and 1000–1800 K for auto-ignition were used. The molecular transport properties and thermochemistry have been implemented using TRANSPORT [19] and CHEMKIN-II [20], respectively; these have been interfaced with the underlying CFD code [21].

2.3. Soot formation

Soot formation is a complex process and can be divided into several subprocesses: (i) nucleation of soot particles, when they acquire characteristics different from the gas phase; (ii) surface growth/oxidation of soot particles due to reactions with the gas phase; and (iii) particle coagulation/aggregation due to collisions between soot particles. All of these processes occur simultaneously and need to be modeled accurately [22].

2.3.1. Soot kinetics

Soot kinetics refers to interaction of soot particles with the surrounding gas phase. It includes soot nucleation, soot surface growth/oxidation and growth due to condensation of polycyclic aromatic hydrocarbons (PAHs). It has been reported that PAH condensation is negligible for atmospheric-pressure ethylene–air flames [2,11]. A simplified nucleation mechanism based on local acetylene (C_2H_2) concentration proposed by Lindstedt and coworkers [10,11,23] is used here. The model can be written as

$$R_N=2\frac{N_A}{C_{\min}}k_N(T)[C_2H_2]. \tag{5}$$

Here R_N is the rate of nucleation of soot particles, N_A is Avogadro's constant, $C_{\min}$ is the number of carbon atoms in the smallest PAH which coagulates into a dimer to form the incipient soot particle, $[C_2H_2]$ is the molar concentration of acetylene and $k_N(T)=0.63\times10^4\exp(-21,000/T)$ is the rate coefficient.

Table 1
Soot surface growth/oxidation mechanism

No.	Reaction	References
1	$C_s + H \rightleftharpoons C_s^* + H_2$	[1,9]
2	$C_s + OH \rightleftharpoons C_s^* + H_2O$	[1,9]
3	$C_s^* + H \rightarrow C_s$	[9]
4A	$C_s^* + C_2H_2 \rightarrow C_s + H$	[9]
4B	$C_s^* + C_2H_2 \rightarrow C_s^* + H$	[24]
5	$C_s^* + O_2 \rightarrow 2CO + \text{products}$	[9]
6	$C_s + OH \rightarrow CO + \text{products}$	[9,25]

Soot surface growth models have been an active area of research for several decades [26]. Frenklach and Wang [9,27] postulated a chemical similarity between the chemical reactions taking place on the soot particle surface and those for large PAH molecules . This mechanism is termed surface hydrogen-abstraction–acetylene-addition (HACA), and is consistent with the findings of Harris and Weiner [28], who determined that acetylene dominates surface growth in their flames. Soot surface oxidation is due to attack by OH radicals and oxygen [25]. Table 1 summarizes key reactions included in the surface-HACA mechanism. In Table 1, $\rightarrow$ indicates an irreversible reaction and $\rightleftharpoons$ denotes a reversible reaction, C_s denotes a soot particle and C_s^* is a soot radical. The kinetic rate coefficients for each of the reactions and other details can be found in the references listed in the table. Two variants for the acetylene-addition reaction (4A versus 4B) are shown. Reaction 4A corresponds to depletion of surface radical sites during acetylene-addition, and has been used in laminar premixed flames with success [1]. Reaction 4B corresponds to conservation of surface radical sites during acetylene addition, and is used in the current study. The choice is supported by a detailed assessment of different soot submodels combined with various gas-phase chemistry mechanisms [2]. Wang et al. [24] have pointed out that, in reality, the surface radical sites are neither completely conserved nor completely depleted during the acetylene-addition step.

2.3.2. Soot particle dynamics

Soot particle dynamics refers to interactions between soot particles, and can be treated in different ways. These include the method of moments where one solves for the moments of the particle-size distribution function (PSDF) [29], and sectional methods [30] where the PSDF is divided into discrete sections by average particle size. Here a method of moments with interpolative closure has been used. Three-to-six moments have been found to be sufficient in previous modeling studies of laminar premixed flames [1,2,9] and opposed-flow diffusion flames [2,24]. The method of moments can be extended to aggregation of soot particles into mass fractals [31]. Since the current study is limited to atmospheric-pressure flames, it is expected that soot particles will remain primarily spheroidal; hence aggregation is not considered. The concentration moments of the PSDF are given by,

$$M_r = \sum_{i=1}^{\infty} m_i^r N_i, \quad r = 0, 1, 2, \ldots, \infty. \tag{6}$$

Here M_r is the rth moment, m_i is the mass of each particle of size-class i, and N_i is the number of particles of size-class i per unit volume. Thus N_i represents the entire PSDF. For $r = 0, M_0 = \sum_{i=1}^{\infty} N_i$ is the total particle number density. For $r = 1, M_1 = \sum_{i=1}^{\infty} m_i N_i$ is the total mass of soot particles per unit volume, and the soot volume fraction is given by $f_v = M_1/\rho_s$, where ρ_s is the soot density. Higher-order moments lack simple physical interpretations but are needed for accuracy. The knowledge of all integer moments ($r = 0, \ldots, \infty$) is equivalent to the knowledge of the PSDF itself. However, most of the principal properties for the particle ensemble can be deduced from the first few moments. Here the first six moments (M_0–M_5) are retained in the formulation. The contributions of nucleation, coagulation, and surface reactions to each moment can be derived from population balance equations and isolated [29]:

$$\frac{dM_r}{dt} = \underbrace{R_r}_{\text{Nucleation}} + \underbrace{G_r}_{\text{Coagulation}} + \underbrace{W_r}_{\text{Surface reactions}}. \tag{7}$$

Surface reactions W_r are due to interaction of soot particles with the surrounding gas-phase species. For spherical particles, the corresponding source terms in the equation for rth moment can be written as [9,29]

$$W_r = k_{sg} C_g \alpha \chi_s \pi \left(\frac{6 m_C}{\pi \rho_s}\right)^{2/3} M_0 \sum_{k=0}^{r-1} \binom{r}{k} \Delta^{r-k} \mu_{r+2/3}, \quad r = 1, 2, \ldots, \tag{8}$$

where k_{sg} is the kinetic rate coefficient for reaction with gas g, C_g is the molar concentration of the gas species, α is a steric factor as explained below, χ_s is the nominal number density of surface radical sites, Δ is the number of carbon atoms added/removed from the soot particle due to reaction with gas g, m_C is the mass of the carbon atom, $\mu_r = M_r/M_0$ is the reduced fractional moment of the PSDF and ρ_s is the density of soot (1.8 g/cm^3 [9]). Here χ_s is the number density of surface radical sites determined from the number density of total surface sites, which in turn is estimated to be $\chi_{\text{all}} \simeq 2.5 \times 10^{15}$ cm^{-2} [27]. A kinetic steady-state approximation is then used to obtain the total radical sites available on the particle for reactions with gas-phase species: $\chi_s = K_{\text{steady}} \chi_{\text{all}}$ [9]. The factor α is the fraction of the surface sites available for chemical reactions, and was introduced by Frenklach and Wang [27] to account for the differences between the soot surface growth rates in low-and high-temperature flames. It was suggested that α quantifies the changing morphology of the soot particle surface as the soot particle travels in the post-flame region, and that the extent of this change is dependent on the particle surface temperature. The physical rationale [1] is that α considers the growing soot surface to have "graphitic" edges amenable to chemical reactions, but some parts are comprised of nonreactive basal aromatic planes. The functional form for α has been evolving over the years, starting with constant values [9,32] to a temperature-dependent value used by Appel et al. [1]:

$$\alpha = \tanh[a(T)/\log \mu_1 + b(T)]. \tag{9}$$

By comparing experimental results from seven laminar premixed flames from different investigators, Appel et al. were able to deduce $a(T)$ and $b(T)$ as functions of local temperature T.

2.4. Turbulence–chemistry interactions

Composition PDF methods are a class of transported PDF methods, where physical scalars including temperature (or absolute enthalpy) and species concentrations are treated as random variables (see [33,34] and references therein). The joint PDF of these scalars is then a function of spatial location $\underline{x}$ and time t. The composition PDF transport equation can be written as [33],

$$\begin{aligned}
&\frac{\partial \mathscr{F}}{\partial t} + \frac{\partial}{\partial x_i}[\widetilde{u}_i \mathscr{F}] + \frac{\partial}{\partial \psi_\alpha}[S_{\alpha,\text{reac}}(\underline{\psi})\mathscr{F}] - \delta_{\alpha s} \\
&\quad \times \frac{\partial}{\partial \psi_\alpha}\left[\frac{4\pi \int_0^\infty \kappa_\eta(\underline{\psi}) I_{b\eta} d\eta}{\rho} \mathscr{F}\right] \\
&\quad = -\frac{\partial}{\partial x_i}\left[\left\langle u_i'' | \underline{\psi} \right\rangle \mathscr{F}\right] + \frac{\partial}{\partial \psi_\alpha}\left[\left\langle \frac{1}{\rho} \frac{\partial J_i^\alpha}{\partial x_i} | \underline{\psi} \right\rangle \mathscr{F}\right] - \delta_{\alpha s} \\
&\qquad \times \frac{\partial}{\partial \psi_\alpha}\left[\left\langle \frac{\int_0^\infty \kappa_\eta(\underline{\psi}) G_\eta d\eta}{\rho} | \underline{\psi} \right\rangle \mathscr{F}\right].
\end{aligned} \tag{10}$$

In Eq. (10) $\mathscr{F}$ is the mass density function. Summation is implied over repeated indices i and α within each term with i and α representing physical and composition space, respectively. $\delta_{\alpha s}$ is the Kronecker delta function, subscript s denotes the absolute enthalpy equation, κ_η is the spectral absorption coefficient of the participating medium, $I_{b\eta}$ is the spectral Planck function, η is the wavenumber and G_η is the spectral incident radiation from all directions (total solid angle of 4π) $G_\eta = \int_{4\pi} I_\eta d\Omega$, I_η is the spectral radiative intensity obtained by solving the radiative transfer equation. The notation $\langle A|B\rangle$ denotes the conditional probability of event A given that B occurs.

Terms on the right-hand side of Eq. (10) must be modeled. The first two terms represent transport in physical space due to turbulent velocity fluctuations and transport in composition space due to molecular transport (mixing), respectively. Turbulent transport is usually modeled using a gradient-diffusion hypothesis.

$$\left\langle u_i'' | \underline{\psi} \right\rangle \mathscr{F} = -\Gamma_t \frac{\partial}{\partial x_i}\left(\frac{\mathscr{F}}{\langle\rho\rangle}\right). \tag{11}$$

The turbulent diffusivity Γ_t is derived from dimensional analysis and other considerations [34], as

$$\Gamma_t = C_\mu \langle\rho\rangle \sigma_\phi^{-1} k^2/\varepsilon = \mu_T \sigma_\phi^{-1}, \tag{12}$$

where μ_T and σ_ϕ are, respectively, the modeled turbulent diffusivity (e.g., obtained from the standard two-equation k–ε model) and a turbulent Schmidt or Prandtl number. The second term on the right-hand side of Eq. (10), corresponds to the molecular mixing. Several mixing models have been proposed [34]. In the current work, the Euclidean Minimum Spanning Tree (EMST) model by Subramaniam and Pope [35] is used. EMST has been shown to perform better than other popular models in nonpremixed turbulent flames [36]. The third term on the right-hand side of Eq. (10) is the radiative absorption including closure for absorption TRI, and will be discussed later (Section 2.5).

Lagrangian particle Monte Carlo methods have been developed to solve modeled PDF transport equations [34]. The basic idea is to represent the PDF by a sufficiently large number of notional particles. The mean quantities at any point are estimated as an ensemble average over the particles in a sufficiently small neighborhood. By its nature, the particle tracking method is grid-free; however, in general, a grid is required to extract the statistics of the scalars at discrete locations. Here a consistent hybrid Lagrangian particle/Eulerian mesh solution algorithm has been used [21,37–40]. The composition PDF method has been extended to include soot scalars (moments) as part of the composition space, thereby capturing the effects of turbulent fluctuations on the highly nonlinear soot subprocesses.

2.5. Radiation

Radiation heat transfer plays an important role in many turbulent flames, and is governed by a complex integro-differential radiative transfer equation (RTE) in five dimensions [13]. In addition, the spectral behavior of the absorption coefficient of the medium depends on its composition and local concentrations of selectively absorbing/emitting combustion gases such as water vapor, carbon dioxide and particulate matter such as soot [41,42]. The radiative source term in the absolute enthalpy equation represents the local net volumetric gain of thermal energy due to both emission and absorption, and can be expressed as [13]

$$S_{\text{rad}} = -\nabla \cdot \underline{q}^R = \int_0^\infty \kappa_\eta \left(\int_{4\pi} I_\eta d\Omega - 4\pi I_{b\eta} \right) d\eta, \tag{13}$$

where $\underline{q}^R$ is the radiative heat flux, $\kappa_\eta = \kappa_\eta(\underline{Y}, T, p)$, is the spectral absorption coefficient of the radiating medium (mixture), which may be a function of temperature T and species concentrations (expressed as mass fractions $\underline{Y}$) of the radiating medium. Here I_η is the spectral radiative intensity, and $I_{b\eta}$ is the Planck function or spectral blackbody intensity. The subscript η denotes spectral dependence and Ω is the solid angle. To determine I_η it is necessary to solve the radiative transfer equation (RTE) and this can be done using various methods, including: (i) spherical harmonics methods [43,44]; (ii) the discrete-ordinates methods [45]; or (iii) photon Monte Carlo (PMC) methods [46–48]. A powerful feature of the PMC methods is their ability to handle complex problems with relative ease.

2.5.1. Turbulence–radiation interactions

The absorption coefficient κ_η depends nonlinearly on both species concentrations and the temperature. Therefore the mean of the product of κ_η and $I_{b\eta}$ is not equal to the product of their means:

$$\langle \kappa_\eta I_{b\eta} \rangle = \langle \kappa_\eta \rangle \langle I_{b\eta} \rangle + \left\langle \kappa_\eta' I_{b\eta}' \right\rangle \neq \kappa_\eta(\tilde{\underline{Y}}, \tilde{h}) \langle I_{b\eta} \rangle, \tag{14}$$

$$\langle I_{b\eta} \rangle \neq I_{b\eta}(\tilde{T}), \tag{15}$$

and similarly,

$$\langle \kappa_\eta I_\eta \rangle = \langle \kappa_\eta \rangle \langle I_\eta \rangle + \left\langle \kappa_\eta' I_\eta' \right\rangle \neq \kappa_\eta(\tilde{\underline{Y}}, \tilde{h}) \langle I_\eta \rangle. \tag{16}$$

The essence of TRI modeling is to accurately estimate the left-hand sides of Eqs. (14) and (16). In these equations, $\langle \kappa_\eta' I_\eta' \rangle$ represents the correlation between the fluctuating absorption coefficient and spectral incident intensity, and $\langle \kappa_\eta' I_{b\eta}' \rangle$ represents the correlation between the fluctuating absorption coefficient and the local blackbody intensity. Following Li [49], these two correlations are loosely defined as absorption coefficient–incident intensity correlation and absorption coefficient–black body intensity (Planck function) correlation, respectively.

2.5.2. Photon Monte Carlo method

For combustion applications where joint PDF methods [34] are used, the medium often is represented by notional particles, and traditional Monte Carlo ray-tracing schemes developed for continuous media [13] cannot be used. Recently, Wang and Modest [50] developed several emission and absorption schemes for media represented by discrete particles. The PMC simulates the process of emitting radiation by releasing representative photon bundles (rays) in random directions, which are traced until they are absorbed (completely) in the medium or escape from the computational domain. An energy-partitioning scheme, which reduces statistical error, compared to standard Monte Carlo [13] is used. In media represented by discrete particles, the ray energy is distributed over all the particles with which the ray interacts when the energy-partitioning method is employed [50].

A fundamental assumption is that the instantaneous particle field can be regarded as a snapshot of a turbulent flow-field [48]. The PMC method can, then, be employed to evaluate both the local emission ($\langle 4\pi\kappa_\eta I_{b,\eta} \rangle$) and the absorption of incident radiation ($\langle \kappa_\eta I_\eta \rangle$) exactly without further assumptions. Emission is fundamentally closed using the one-point PDF and does not require modeling. Therefore it is evaluated correctly even when considering optically thin radiation. The PMC model allows accurate determination of both emission and absorption TRI within statistical limits and does not need any other modeling assumptions (such as negligible absorption TRI, etc.). The effects of TRI may be different for sooting and nonsooting flames. In the case of nonsooting flames, it has been shown that TRI enhances radiative emission and radiative loss, and causes a decrease in the flame temperature. There have been fewer studies for sooting flames with respect to effects of TRI [51]. In sooting flames the TRI will additionally depend on correlations between temperature fluctuations and soot concentration fluctuations, which may either be positive or

negative, depending on the values of temperature, soot concentration, wavelength and turbulent intensity.

2.5.3. Spectral photon Monte Carlo

Recently Wang and Modest [52,53] proposed a PMC coupled with both full-spectrum k-distributions (FSK) [54] and with line-by-line (LBL) calculations. They showed that the computational cost for both methods was comparable and was acceptable for statistically stationary flames. Thus, with this method it is possible to attain line-by-line spectral accuracy for radiative calculations in reacting flows. Key elements of the spectral PMC are outlined here [13]. The probability of a photon being emitted in a differential wavenumber interval $d\eta$ is proportional to the Planck function weighted by the spectral absorption coefficient:

$$\text{Probability}(\eta \leqslant \eta' \leqslant \eta + d\eta) \propto \kappa_\eta I_{b\eta} d\eta. \tag{17}$$

To simulate emission from a nongray gas using photon bundles, one can statistically map the wavenumber for a given gas-phase species α to a uniform random number $R_{\eta,\alpha} \in [0,1)$ such that,

$$R_{\eta,\alpha} = \frac{\int_0^\eta \kappa_{\eta,\alpha} I_{b\eta} d\eta}{\int_0^\infty \kappa_{p,\eta,\alpha} I_{b\eta} d\eta} = \frac{\int_0^\eta \kappa_{p,\eta,\alpha} I_{b\eta} d\eta}{\int_0^\infty \kappa_{p,\eta,\alpha} I_{b\eta} d\eta} = \frac{\pi}{k_{p,\alpha}\sigma T^4} \int_0^\eta \kappa_\eta I_{b\eta} d\eta, \tag{18}$$

where $\kappa_{p,\eta,\alpha} = \kappa_{\eta,\alpha}/p_\alpha$ is the pressure-based spectral absorption coefficient, and p_α is the partial pressure of species α; $k_{p,\alpha}$ is the Planck-mean pressure-based absorption coefficient. Since Eq. (18) is an implicit relationship between the random number and the wavenumber, it is convenient to tabulate this relationship in a database and invert random numbers to obtain the emission wavenumbers for the photon bundles.

When dealing with mixtures of multiple absorbing-emitting gases, and assuming that absorption coefficients are additive, one can derive a random number relationship between wavenumber for the mixture and a uniform random number $R_\eta \in [0,1)$. It can be shown that [52]

$$R_\eta = \frac{\sum_\alpha \chi_\alpha k_{p,\alpha} R_{\eta,\alpha}}{\sum_\alpha \chi_\alpha k_{p,\alpha}}, \tag{19}$$

where $\chi_\alpha = p_\alpha/p$ is the mole fraction of species α, p is the total pressure of the mixture, and $R_{\eta,\alpha}$ are the species random numbers. The relationship between η and R_η is implicit and the mapping between R_η to η requires iterations. For efficient computations it is possible to pretabulate $R_{\eta,i}$ versus η and $\kappa_{p,\eta,i}$ versus η relationships, then use an interpolation scheme [52]. A similar formulation can be done for the FSK approach [52]. It was found that the numerical effort for PMC was similar for FSK and LBL. Here the LBL approach is used for carbon dioxide, water vapor and soot.

2.5.4. Soot radiative properties

Soot particles are assumed to be spherical and small compared to the wavelengths of interest; this limits the applicability to atmospheric or slightly higher pressures. Rayleigh theory is used to obtain expressions for both the absorption and scattering coefficients of the soot particles [13]. Light scattering was not considered as it is negligible compared to absorption, in the small particle limit. For small particles, the spectral absorption coefficient of soot is evaluated as [13]:

$$\kappa_\lambda = \frac{36\pi n k}{(n^2 - k^2 + 2)^2 + 4n^2k^2} \frac{f_v}{\lambda}, \tag{20}$$

where f_v is the soot volume fraction, λ is the wavelength and n and k are components of the complex index of refraction of soot $m = n - ik$. Functional forms of n and k for soot particles as a function of wavelength proposed by Chang and Charalampopoulos [55] are used here. Based on Eq. (20), the random number relationships for soot can be calculated similar to Eq. (18) as

$$R_{\eta,s} = \frac{\pi}{k_{p,s}\sigma T^4} \int_0^\eta \kappa_{\eta,v,s} I_{b\eta} d\eta, \tag{21}$$

where the subscript s denotes soot, $\kappa_{\eta,v,s} = \kappa_{\eta,s}/f_v$ is the soot-volume-fraction-based spectral absorption coefficient, and $k_{p,s}$ is the corresponding Planck-mean absorption coefficient. Thus, the random number relationship for mixtures of nongray gases and soot can be calculated similar to Eq. (19) as

$$R_\eta = \frac{P\sum_i \chi_i k_{p,i} R_{\eta,i} + f_v k_{p,s} R_{\eta,s}}{P\sum_i \chi_i k_{p,i} + f_v k_{p,s}}, \tag{22}$$

where subscript i denotes participating gaseous species, and s denotes soot. Similar to the approach that was used in the gas-phase random-number databases, the mappings between $R_{\eta,s}$ versus η and $\kappa_{\eta,v,s}$ versus η can be pretabulated, and then used as necessary. Additional details of this approach can be found in [52,53].

2.6. Model summary

Table 2 lists all the physical/empirical models used in the turbulent reacting flow simulation. Most of these models have one or more "model constants". In the current study, all model parameters have been kept constant for all the flame simulations. None

Table 2
Summary of submodels used in the current study.

Quantity	Model	Adjustable parameters	Values	References
Turbulent Reynolds stress	k–ε	C_μ, $C_{\varepsilon1}$, $C_{\varepsilon2}$, σ_k, σ_ε	$C_\mu = 0.09$, $C_{\varepsilon1} = 1.44$, $C_{\varepsilon2} = 1.92$ (standard)	[57]
Turbulent species, enthalpy fluxes	Gradient diffusion + k–ε	Turbulent Schmidt (Sc_T) and Prandtl (Pr_T) numbers	$Sc_T = 0.7$, $Pr_T = 1$ (standard)	[57]
Chemical source terms (closure)	Transported PDF method	Mixing models	EMST ($C_\phi = 2$)	[58]
Gas-phase chemistry	33-species, 205-reactions (QLY33)	None	–	[16,18]
Soot model	Method of moments	Nucleation, surface reactions, radical conservation	Model 32 from [2]	[2]
Soot scalar source terms (closure)	Transported PDF method	Mixing model	No mixing	[59]
Gas-phase radiative properties	Line-by-line databases: H_2O, CO_2	None	Neglect CO and fuel radiation	[13]
Soot radiative properties	Absorption coefficient based on [55]	Complex index of refraction, scattering	$m = n(\eta) - ik(\eta)$, Rayleigh scattering (negligible)	[13,55]
RTE solver	Full nongray photon Monte Carlo	Cone opening angle, number of rays, energy partitioning	Based on [53] and PDF settings	[53]
TRI (closure)	Emission and absorption TRI	Within statistical limits		[53]

of the model parameters are "tuned" for any particular flame to achieve better agreement. In spite of the moderate soot levels of the flames, turbulence radiation interactions (TRI) were found to be important. The radiation characteristics of these flames are discussed in detail in [56].

3. Flame configurations

Several turbulent jet flames have been simulated (Table 3) for a range of jet Reynolds numbers, and with two different fuels: pure ethylene fuel or a blend of 90% methane–10% ethylene by volume. Flames I and II are moderately sooting ethylene flames with peak soot volume fraction of approximately 1.5 ppm. Flames III–VI burn a 90% methane–10% ethylene blend and have much lower sooting propensities. Peak soot volume fractions in these flames are approximately 0.2 ppm, in spite of the fact that the residence times for these flames are much larger compared to Flames I and II.

3.1. Experimental data

Flame I is a turbulent jet flame studied experimentally by Coppalle and Joyeux [60]; the jet Reynolds number is 11800. The mean temperature and soot volume fractions were measured using two-color pyrometry and extinction measurements, respectively. Particle temperatures were measured using two-color pyrometry. Probe measurements in relatively low-soot regions showed good agreement with the mean temperatures that were measured using pyrometry.

Kent and Honnery [61] studied ethylene/air jet flames with Reynolds numbers from ~ 7500 to $\sim 15,000$. Extinction measurements were carried out along secants, and radial soot volume fraction profiles were estimated using an Abel inversion technique [63]. A consequence of this inversion technique is that the reported soot volume fractions can have an especially high degree of uncertainty near the axis of the flame. The degree of uncertainty, however, was not quantified. Temperatures were measured using uncoated thermocouples, and a radiation correction was applied using a surface emissivity of 0.2. The authors also reported a modeling study for these flames using a state relationship between local mixture fraction and soot volume fraction. Although qualitative agreement was reported, the model results did not match well with experimentally measured values for soot volume fractions. They concluded the study by re-iterating that the time scales for soot formation are such that a state relationship with local compositions cannot adequately predict soot formation.

Turns and coworkers [62,64–66] undertook detailed characterization of turbulent jet flames with oxygen enrichment. They conducted a number of experiments to understand how key parameters affect the soot, radiation and pollutant-emission characteristics of jet flames over a range of oxygen indices from 21% (air oxidizer) to 100% (pure O_2 oxidizer). Fuel issued from a jet with inner diameter 3 mm, into a low-velocity oxidizer stream. The fuel jet velocities (jet Reynolds numbers) were varied to understand effects of turbulence levels and residence times on measured quantities. Several fuel types including propane, natural gas (94% methane), and methane–ethylene mixture (90–10% by volume) were used. Endrud [62] reported experimental data which was later extended and used by Wang [66] in developing comprehensive modeling strategies for turbulent jet flames [41,42]. Line-of-sight laser-extinction measurements were used to determine an equivalent soot volume fraction at different axial locations. The equivalent soot volume fraction is given by

$$Fv^* = \frac{1}{d_j}\int_{-\infty}^{\infty} Fv(r)dr = \frac{\lambda}{6\pi d_j \mathrm{Im}\left(\frac{m^2-1}{m^2+2}\right)} \ln\frac{I}{I_0}, \tag{23}$$

where d_j is jet diameter, λ is the wavelength of the laser used for measurement, $m = n - ik$ is the complex index of refraction of soot and I/I_0 is the measured attenuation (extinction) of the intensity as the beam passes through the flame. It was argued by Wang et al. [64], that the equivalent soot volume fraction is an easily reproducible global measurement; in the absence of simultaneous detailed measurements of soot volume fraction, velocities and temperature, the equivalent soot volume fraction is a more precise way to differentiate among sooting characteristics compared to Abel-inversion technique to get radial profiles of soot volume fractions. Radiation measurements were made using a wide-angle (150°) window. Radiative heat flux measurements were made at 100 mm intervals along the wall, and then integrated to determine the total radiative heat loss. Duct walls were coated with high-temperature infrared-black paint. Radiant heat loss as a fraction of the total chemical heat release rate was also reported [62,64].

Table 3
Turbulent flames simulated.

Flame	Fuel (by volume)	Oxidizer	Reynolds number	References
I	Pure C_2H_4	Air	11,800	[60]
II	Pure C_2H_4	Air	15,100	[61]
III	90% CH_4–10% C_2H_4	Air	6700	[62]
IV	90% CH_4–10% C_2H_4	30% O_2	6700	[62]
V	90% CH_4–10% C_2H_4	40% O_2	6700	[62]
VI	90% CH_4–10% C_2H_4	55% O_2	6700	[62]

4. Results and discussion

A three-dimensional wedge-like grid system is employed to simulate the axisymmetric flames by applying periodic boundary conditions on the lateral surfaces, with a wedge angle of 10°; the dimensions in x-(radial) and z-(axial) directions are $30d_j$ and $250d_j$, respectively. The grid is fine near the fuel jet to accurately resolve large local gradients in the mixing region, and is coarser in the coflow air region and downstream to save computational time. With composition PDF methods it has been found that approximately 30 particles per cell are sufficient to resolve the turbulent fluctuations in the flame. Approximately 100,000 photon bundles at every time-step were found to be sufficient for statistically stationary configurations. Equilibrium chemistry is used in a small region close to the fuel jet exit, to stabilize the flame.

The composition space contains 40 scalars (33 species, first six moments of the soot PSDF and mixture specific enthalpy). A typical simulation time is four-to-five days on 16 processors (3.0 GHz, Intel Quad Core Processors, 2MB L2 Cache per core and a GB ethernet interconnect). For Flame IV (Typical of the simulations reported here), 73% of the CPU time was spent on gas-phase chemistry (and soot), 24% was for the Photon Monte Carlo solver, 2% was for the EMST mixing model and 1% was for the remainder of the simulation. Greater than 90% parallel efficiency was achieved for up to 128 processors. Since these simulations were performed, significant improvements have been made in the PMC algorithms, in particular, to the point where chemistry and soot account for greater than 90% of the computational effort.

4.1. Results for Flame I

Transient simulations are carried out using a computational timestep of $\Delta t = 50\,\mu s$ until a statistically steady solution is reached. Fig. 1 shows the converged steady-state contours of the mean temperature and mean soot volume fraction. The contours show reasonable distribution of soot consistent with the experimentally-observed flame structure. For example, the peak soot is on the fuel-rich side, as expected.

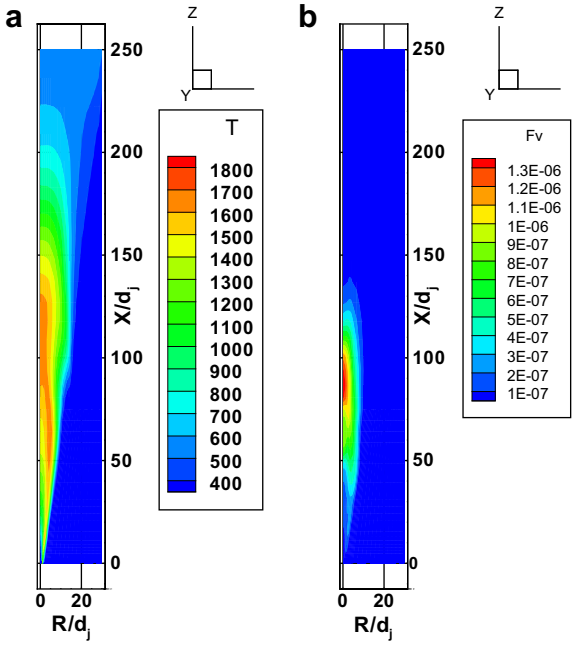

Fig. 1. Computed mean temperature and mean soot volume fraction contours for Flame I.

The computed centerline mean temperature profiles for Flame I obtained without soot radiation, and with soot radiation using either the optically thin approximation or the PMC are shown in Fig. 2. Soot radiation has a large effect on the temperatures and, consequently, on the entire flame structure. The peak centerline mean temperature drops by more than 300 K from 1920 K without soot radiation to 1600 K for optically thin radiation including soot. With optically thin radiation the temperature is under-predicted compared to the experimentally measured value of 1665 K. Optically thin radiation results also predicts lower temperatures in most of the downstream region. This has important implications on soot formation and oxidation rates and therefore on soot profiles. When re-absorption is included the computed peak mean centerline temperature is 1678 K, which is close to the experimental value.

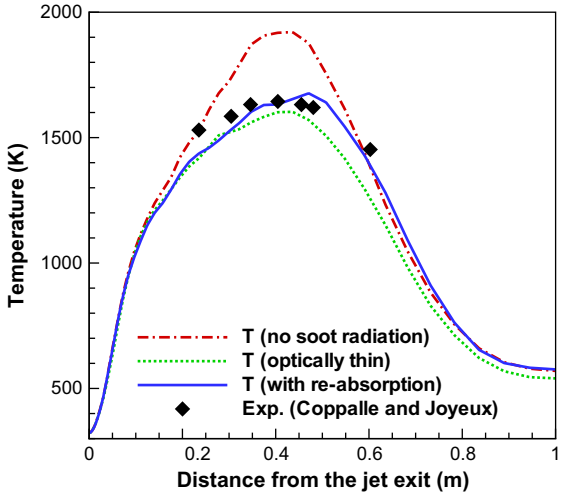

Fig. 2. Measured (symbols) and computed (lines) centerline mean temperature profiles Flame I. Computed profiles are shown for three levels of radiation modeling.

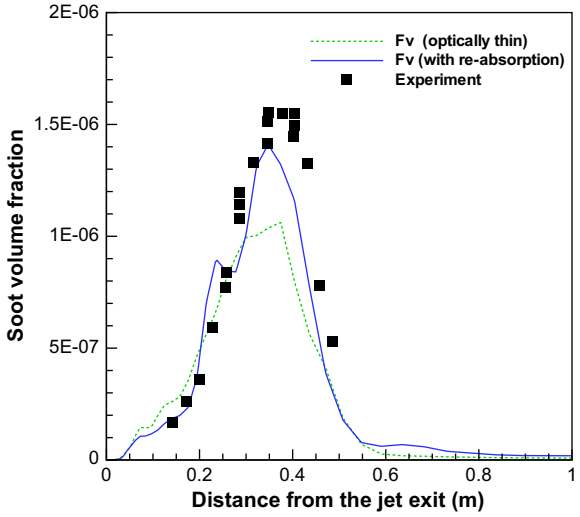

Fig. 3. Measured and computed centerline mean soot volume fraction profiles using optically thin radiation and PMC method for Flame I.

The computed centerline mean soot profiles (for Flame I) are compared with experiment in Fig. 3. The peak axial soot volume fraction is slightly lower than experiments when using both optically thin and PMC (re-absorption) models. Re-absorption results in higher temperatures, which increase both surface growth and oxidation rates, and local conditions dictate the net effect on the soot growth rates. Accounting for re-absorption results in a higher soot formation rate, giving (slightly) better agreement with experiments. Radial soot volume fraction profiles for Flame I at two different axial stations are shown in Fig. 4. The model predictions capture the experimental trends well. Both radiation treatments capture the off-center peak location reasonably well.

4.2. Results for Flame II

Computed centerline mean temperature profile for Flame II is compared with the experiments in Fig. 5. Computed peak mean temperature is 1850 K which is about 70 K higher than the experimental peak temperature of 1778 K. As noted in [61], the uncertainty in measured temperatures is high in presence of soot. The discrepancy between computed and measured temperatures is small in the upstream region, and increases in the region where large amounts of soot are present. The overall trend of temperature drop after the soot peak is captured reasonably well. The computed axial soot volume fraction profile is also shown in Fig. 5.

Kent and Honnery presented the experimental data relative to the position where maximum laser extinction occurred [61]; that location is denoted by x_m. Table 4 compares several global quantities from simulation with the corresponding experimental data.

Computed and experimental radial mean temperature profiles for Flame II at different axial locations are shown in Fig. 6. The axial distances are normalized based on the computed peak-soot location. There is good agreement at the upstream station ($x/x_m = 0.4$), much before the peak soot volume fraction location. Downstream at $x/x_m = 0.7$, the computed temperature is higher at the axis, while it drops faster, than the experiment, away from the axis. Near the peak soot location $x/x_m = 1$, the temperature is over-predicted near the axis, but overall agreement is very encouraging in the radial direction.

Experimental radial mean soot volume fraction profiles for Flame II were obtained by an Abel-inversion of the line-of-sight extinction data based on an assumed complex index of refraction for soot $m_{\text{Flame II}} = 1.94 - 0.54i$. The inversion procedure also

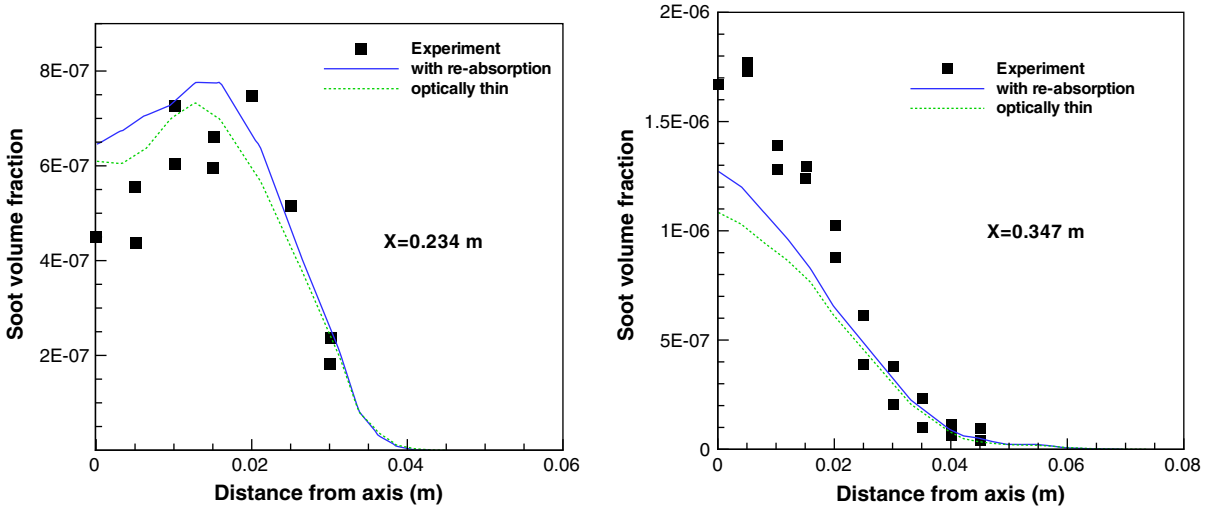

Fig. 4. Measured and computed radial soot volume fraction profiles at two axial stations for Flame I.

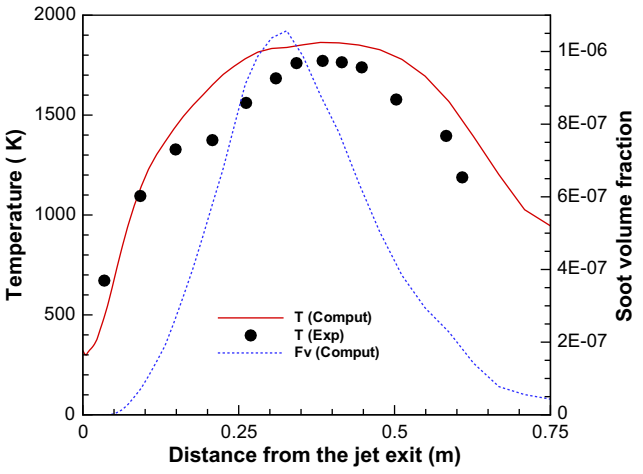

Fig. 5. Centerline mean temperature profiles for Flame II. Dashed line is the computed soot volume fraction.

Table 4
Comparison between computed and experimental values for Flame II.

Description	Experiment	Computation
Peak soot location (x_m) (m)	0.345	0.328
Peak temperature location (m)	0.38	0.37
Peak temperature (K)	1778	1850
Axial peak soot (ppm)	–	1.05

results in an increased uncertainty near the axis [61]. In the current study, the index-of-refraction correlations given by [55] have been used. Hence, the computed data was scaled to be consistent with experimental data. Radial mean soot volume fraction profiles for Flame II at various axial locations are shown in Figs. 7 and 8. The computed soot volume fraction at the upstream station ($x/x_m = 0.4$) shows an off-center peak not seen in the experiment. Prediction of soot levels is within a factor of two over most of the domain. At the downstream location ($x/x_m = 0.7$), the computed soot is within 30% of the experiment, throughout the radial distance.

At the peak soot station $x/x_m = 1$ (Fig. 8), the soot is under-predicted near the axis, while it is over-predicted away from the axis. This could be due to lower oxidation rates in the simulations compared to the experiments, or it may be due to uncertainty of soot measurements near the axis. A similar trend is seen in the downstream station $x/x_m = 1.4$; there the soot is over-predicted by up to a factor of 2.0 away from the axis. This probably is still within the expected accuracy of the models and measurements.

The modeled soot core extends further radially than the experimental data. However, in general, the agreement with the experimental data is very encouraging.

4.3. Results for Flames III–VI

The computed centerline mean temperature profiles for Flames III–VI are shown in Fig. 9. Peak axial mean temperature increases from ~ 1800 K to ~ 2600 K with increasing oxygen content. The increased temperatures have a direct effect on the soot levels and on overall flame structure, as discussed later. In addition, the axial location of the peak temperature shifts upstream with increasing oxygen enrichment as the fuel burns off in shorter distance after exiting the jet. Consequently, the residence times for the flames and the flame length decrease with increasing oxygen enrichment.

For Flames III–VI, Endrud [62] reported a random-error element in the equivalent soot measurements of approximately $\pm 5.0 \times 10^{-7}$, and hence for small soot volume fractions, the signal to noise ratio is very low for reliable measurements. This is the case with Flame III, with standard air as the oxidizer, and also when oxygen concentration is increased beyond 55%. Equivalent soot volume fractions for Flames III–VI are shown in Fig. 10. The peak soot volume fraction is highest at 30% oxygen and drops progressively as the oxygen content is increased. The increase in oxygen has conflicting influences on soot kinetics:

(a) Higher oxygen concentration increases the hydrogen-radical pool (H_2–O_2 chemistry). The hydrogen radicals are very active and result in more radical sites on the soot surfaces, which in turn increases acetylene-addition and hence promotes soot growth (via surface reactions).
(b) Increased oxygen oxidizes the soot precursors as well as the soot that is being formed, thereby reducing the soot formation.

The net effect of oxygen enrichment is therefore determined by the relative importance of these two effects. For relatively low levels of oxygen enrichment, the increasing oxygen results in a larger increase of the hydrogen-radical pool and hence a much enhanced

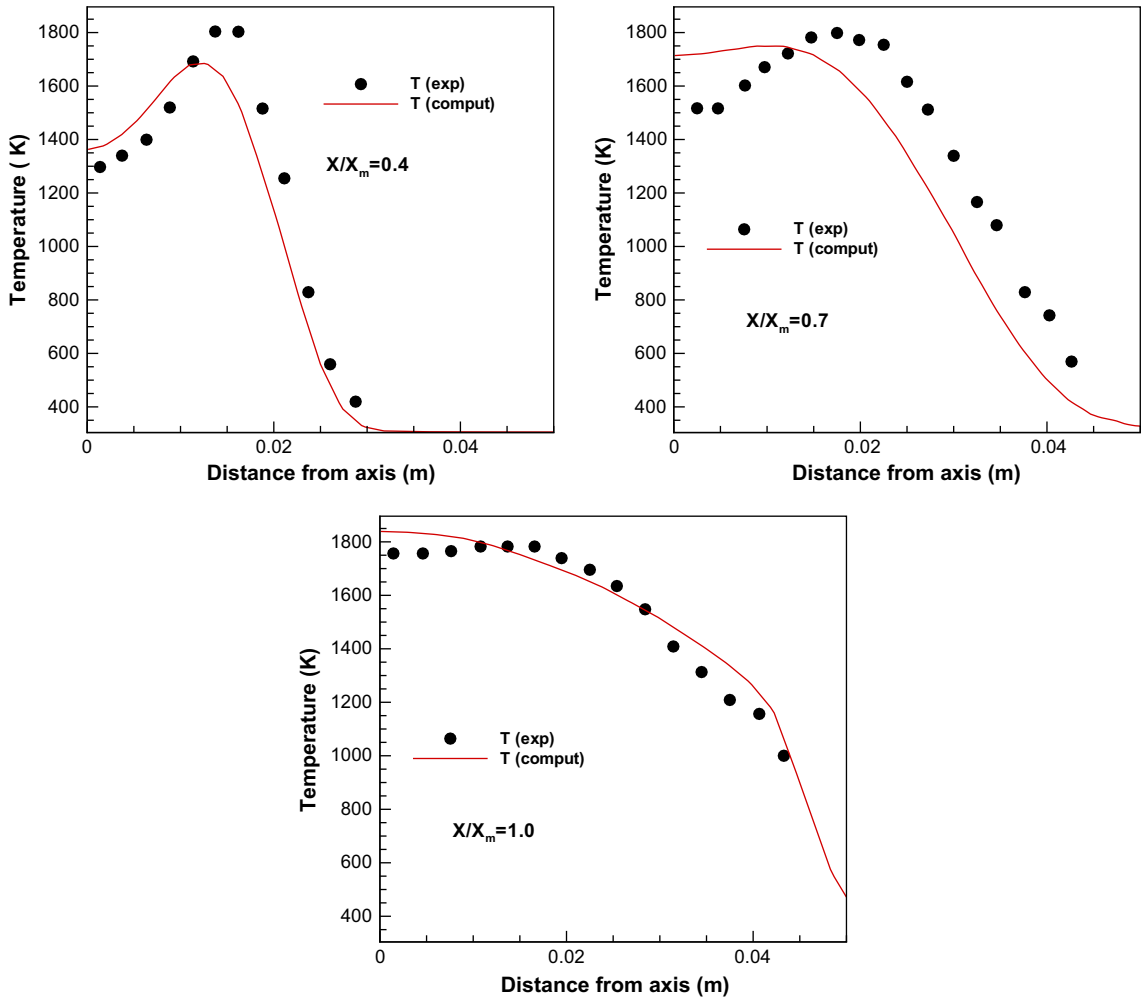

Fig. 6. Measured (symbols) and computed (lines) radial mean temperature profiles at three axial locations for Flame II.

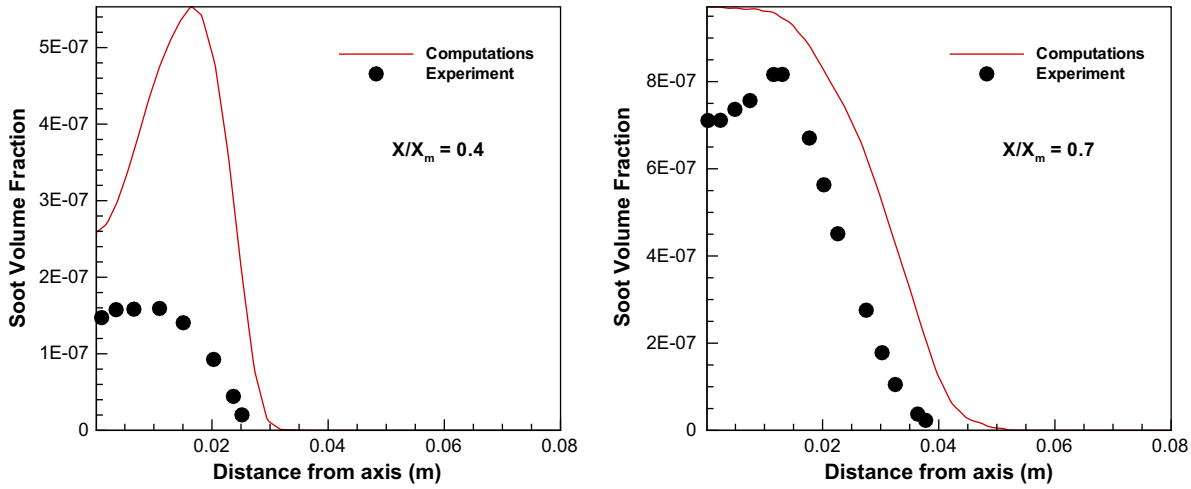

Fig. 7. Measured (symbols) and computed (lines) radial soot volume fraction profiles at the upstream stations for Flame II.

soot growth. For high levels of oxygen enrichment, the increased soot (and soot precursor) oxidation rates dominate.

The computed peak soot location is consistently upstream compared to the experimental data. Soot is under-predicted for Flames IV and V, while slightly over-predicted for Flame VI. It should also be noted that the gas-phase reaction mechanism used was optimized for ethylene (C_2H_4) and may not be appropriate for fuel mixtures with higher percentages of CH_4. Nevertheless the computed soot volume fractions are within 25% of the experiments and the model captures the nonmonotonic variation of soot levels with

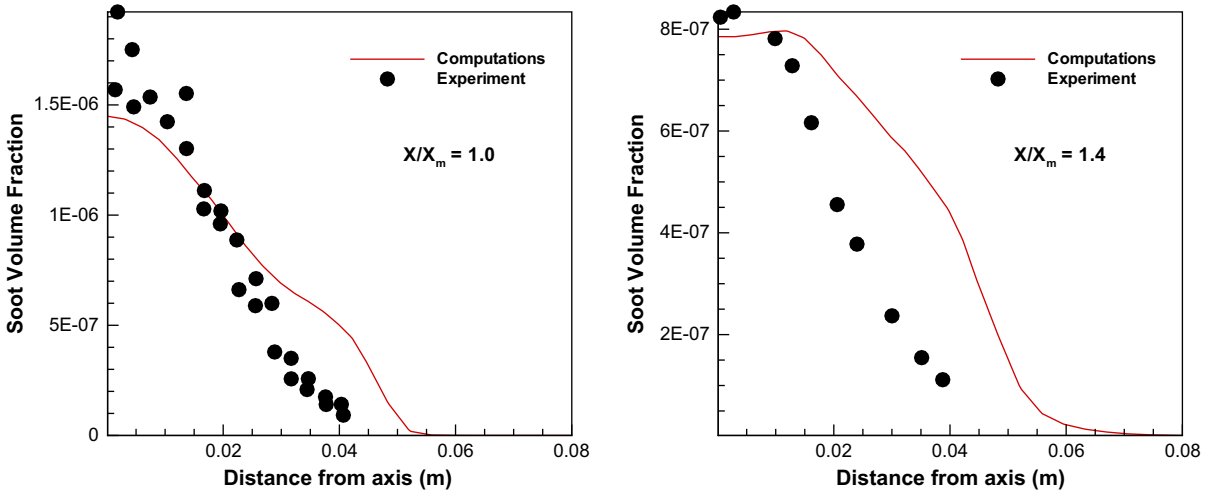

Fig. 8. Measured (symbols) and computed (lines) radial soot volume fraction profiles at the downstream stations for Flame II.

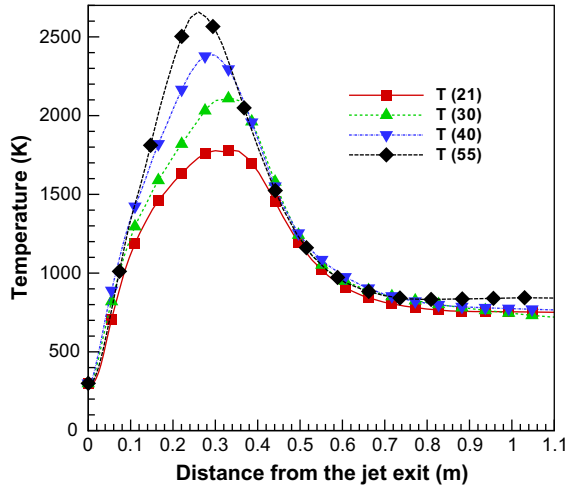

Fig. 9. Computed centerline mean temperature profiles for Flames III–VI with increasing oxygen enrichment in the oxidizer stream.

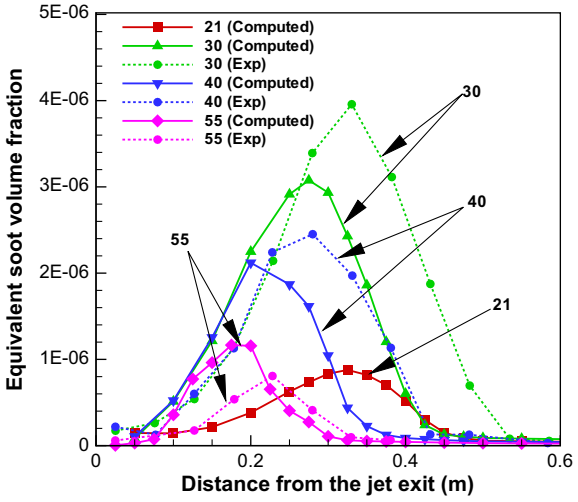

Fig. 10. Computed and measured equivalent soot volume fraction profiles Fv^* for different oxygen indices (Flames III–VI).

oxygen enrichment. This represents a significant advance in state-of-the-art soot modeling in sooting turbulent flames.

Computed and experimental radiative wall fluxes for Flames III–VI are compared in Fig. 11. The peak predicted radiative flux is within ~ 15–20% of measurements in all cases. The radiative emission has a fourth power dependence on the temperature; thus a 20% discrepancy in radiative fluxes would suggest a temperature discrepancy of ~ 5%, if all other quantities are predicted correctly. Similar studies were done by Wang et al. [64] using a Two-Stage Lagrangian (TSL) model for turbulence–chemistry interactions and a combination of the discrete-ordinates (S_2) and P_1 approximation with a gray gas and soot approximation for solving the RTE. For soot modeling, Wang et al. [64] used Model 11 listed in [2]. Although the model captured sooting trends well, the computed soot levels were under-predicted by more than an order of magnitude. Separate studies on prediction of radiative heat transfer using nongray gases and soot, carried out using artificially enhanced soot profiles [41,42] showed limitations of the P_1 method in luminous jet flame configurations. There the optically thick sooting core coupled with optically thin participating gases resulted in an anisotropic intensity distribution which renders P_1-approximation inaccurate. The use of PMC, in this study, results in a much better agreement with experimental data and shows the efficacy of all the underlying models being applied. Higher computed temperatures reported in [64] can also suppress soot formation, thereby affecting the radiative losses from the flame and in general the overall flame structure. Accurately accounting for the turbulence–chemistry interactions is known to reduce the predicted temperatures to a great extent, particularly in jet flames [21,67].

As noted earlier for peak mean soot volume fraction, the computed peak wall fluxes for all Flames III–VI are upstream of the experimental measurements. This discrepancy between the experimental and computed peak location for radiative wall flux increases with increasing oxygen index (Table 5).

4.4. General comments on soot prediction in turbulent flames

Soot, gas-phase chemistry, turbulence and radiation interact strongly in nonlinear ways to determine the overall flame structure. Here Model 32 from [2] has been used for modeling soot formation in turbulent jet flames. This model represents a compromise between computational effort and accuracy. The best performing models from [2] involved larger chemical mechanisms compared to the one use in Model 32. For example, Model 16

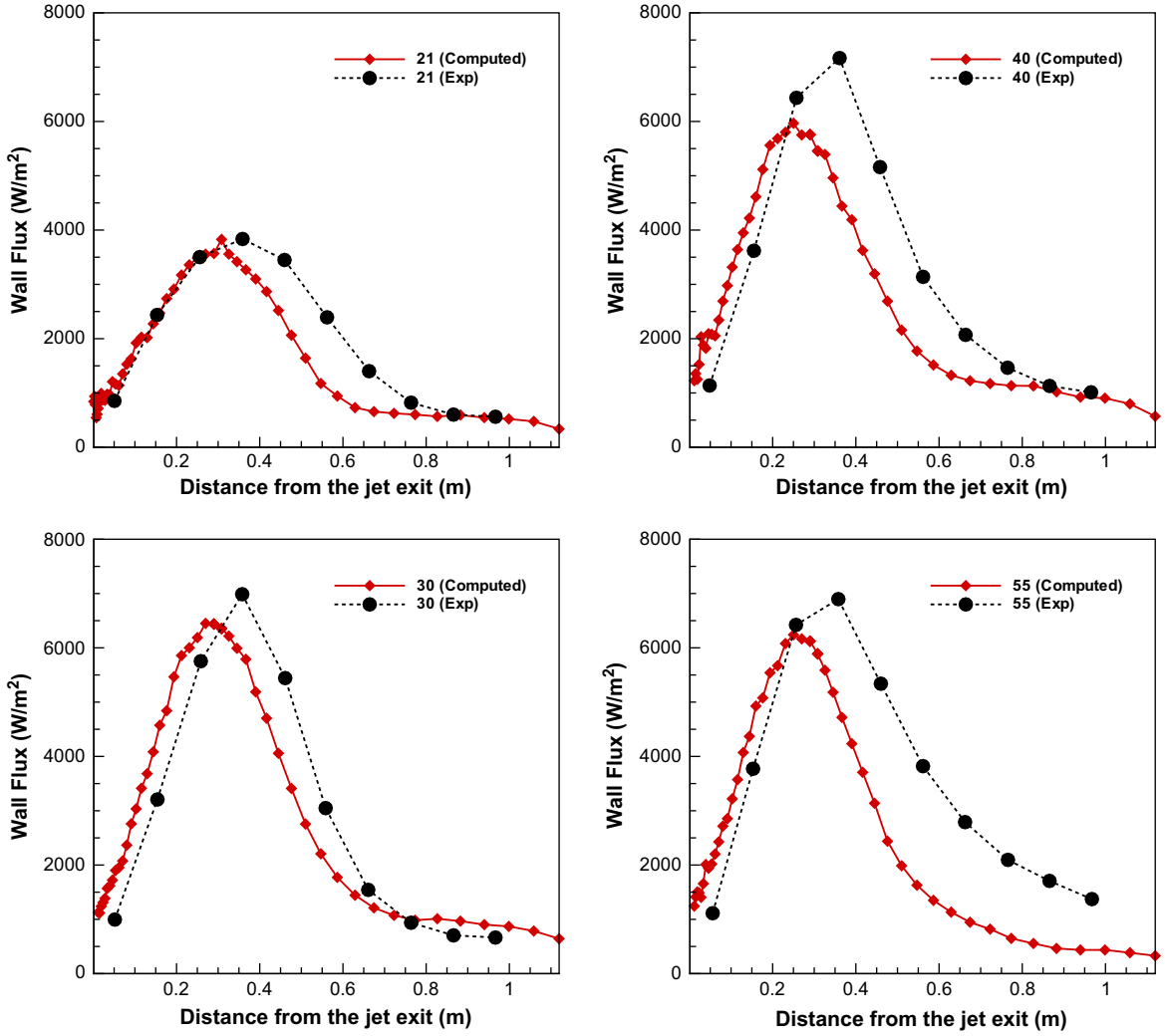

Fig. 11. Computed (symbols) and measured (lines) radiative wall flux for Flames III–VI.

Table 5
Computed and measured location (from jet-exit plane) of the peak wall flux for Flames III–VI.

Flame	Oxygen index	Computed location (m)	Measured location (m)	Difference (m)
III	21	0.306	0.360	0.054
IV	30	0.293	0.360	0.067
V	40	0.262	0.360	0.098
VI	55	0.251	0.360	0.109

contained 100 species, Model 28 contained 70 species. Turbulent flame simulations using these larger mechanisms are being performed in ongoing research. In the meantime, the gas-phase chemistry of Model 32 is the closest of the smaller models to that of Model 28; hence Model 32 was the first to be tested in turbulent flames. This model over-predicted soot for most of the laminar flames that were investigated in [2]; the maximum discrepancy was approximately a factor of 10. However, when applied in turbulent flames the same model predicts soot to within a factor of 1.5–2 for all of the flames that have been studied, irrespective of the fuel-type, jet Reynolds number or sooting propensity.

The most probable explanation for the somewhat different behavior in laminar flames versus turbulent flames may be that the soot particles were modeled as spherical particles with:

i. *Perfect coagulation*: Two spherical particles collide and coalesce completely into a larger spherical particle.
ii. *Uniform surface reactions*: Surface reactions grow the particles while maintaining spheroidal geometry.

For spherical particles, the area-to-volume ratio is $3/r$. In reality, soot particles may have nonspherical geometries with much higher area-to-volume ratios. If nonspherical geometry were considered (for example, aggregation into mass-fractals), the soot model (Model 32 from [2]) would predict higher soot volume fractions due to the higher number of surface-reaction sites. This may explain why soot models that predict soot accurately in laminar flames tend to under-predict soot levels in turbulent flames here. Accounting for soot aggregation into nonspherical mass fractals in the method of moments [31] has been shown to give better agreement in high-pressure laminar flames. The current model can be extended to handle soot aggregation, and this is the subject of ongoing work. Another possibility would be to resolve the soot PSDF using methods like a sectional method, for example. The sectional methods represent the soot PSDF more directly compared to the method of moments. It is expected that they will be able to handle nonspheroidal aggregation into mass fractals more easily compared to the method of moments.

5. Conclusion

A transported PDF method coupled with detailed gas-phase chemistry and soot models, and a photon Monte Carlo radiative transfer equation solver have been applied to luminous turbulent jet flames with Reynolds numbers varying from 6700 to 15100. Two ethylene/air flames and four flames fueled with a 90% methane/10% ethylene (by volume) blend with different levels of oxygen in the oxidizer stream have been simulated. All physical and numerical parameters have been held constant. With the exception of the well-established k–ε turbulence model, all other physical processes are simulated using advanced models. This includes the models for gas-phase chemistry (skeletal-level), soot kinetics, soot-particle dynamics (method of moments with interpolative closure), radiation properties (full spectral treatment for participating gas-phase species and soot), and the effects of fluctuations in composition and temperature (transported PDF method). An advanced RTE solver has been used, that, in combination with the transported PDF method, captures both emission and absorption TRI. Emission TRI was found to be important in all the flames studied, while the absorption TRI was found to be negligible for the laboratory-scale flames [56].

Results show uniformly good agreement between experimental and computed mean temperatures and soot volume fractions. For Flames III–VI, the computed jet spreading rate is slightly high, and this could be corrected by adjusting the coefficients in the turbulence model. The gas-phase chemistry and soot models were validated extensively in laminar flames [2] and used without modifications in the turbulent flames. Although the soot model was validated only in ethylene/air flames, it performs reasonably well even in the oxygen-enriched methane/ethylene flames. Radiative flux measurements are available for Flames III–VI, and the computed fluxes are in good agreement with the experiments. This shows that by following a systematic approach and using state-of-the-art physical models and numerical algorithms, it is possible to capture the complex behavior of a broad range of luminous turbulent flames without adjusting model parameters.

Acknowledgments

This work has been supported by the National Science Foundation under Grant #CTS-0121573 and NASA under Grant #NNX07AB40A. RSM would also like to thank Professor Stephen Turns of The Pennsylvania State University for fruitful discussions.

References

[1] J. Appel, H. Bockhorn, M. Frenklach, Kinetic modeling of soot formation with detailed chemistry and physics: laminar premixed flames of C_2 hydrocarbons, Combust. Flame 121 (1–2) (2000) 122–136.
[2] R.S. Mehta, D.C. Haworth, M.F. Modest, An assessment of gas-phase reaction mechanisms and soot models for laminar atmospheric-pressure ethylene–air flames, Proc. Combust. Inst. 32 (1) (2009) 1327–1334.
[3] S.J. Brookes, J.B. Moss, Predictions of soot and thermal radiation properties in confined turbulent jet diffusion flames, Combust. Flame 116 (4) (1999) 486–503.
[4] I.M. Aksit, J.B. Moss, A hybrid scalar model for sooting turbulent flames, Combust. Flame 145 (1–2) (2006) 231–244.
[5] W. Kolmann, I.M. Kennedy, Application of a soot model to a turbulent ethylene diffusion flame, in: H. Bockhorn (Ed.), Soot Formation in Combustion: Mechanisms and Models, Springer-Verlag, New York, 1994.
[6] M.J. Zimberg, S.H. Frankel, J.P. Gore, Y.R. Sivathanu, A study of coupled turbulent mixing, soot chemistry, and radiation effects using the linear eddy model, Combust. Flame 113 (3) (1998) 454–469.
[7] B. Zamuner, F. Dupoirieux, Numerical simulation of soot formation in a turbulent flame with a Monte Carlo PDF approach and detailed chemistry, Combust. Sci. Technol. 158 (1) (2000) 407–438.
[8] M. Balthasar, F. Mauss, A. Knobel, M. Kraft, Detailed modeling of soot formation in a partially stirred plug flow reactor, Combust. Flame 128 (4) (2002) 395–409.
[9] M. Frenklach, H. Wang, Detailed mechanism and modeling of soot particle formation, in: H. Bockhorn (Ed.), Soot Formation in Combustion: Mechanisms and Models, Springer-Verlag, New York, 1994.
[10] R.P. Lindstedt, S.A. Louloudi, Joint-scalar transported PDF modeling of soot formation and oxidation, Proc. Combust. Inst. 30 (1) (2005) 775–783.
[11] K.M. Leung, R.P. Lindstedt, W.P. Jones, A simplified reaction mechanism for soot formation in nonpremixed flames, Combust. Flame 87 (3–4) (1991) 289–305.
[12] P.E. Desjardin, S.H. Frankel, Two-dimensional large eddy simulation of soot formation in the near-field of a strongly radiating nonpremixed acetylene–air turbulent jet flame, Combust. Flame 119 (1–2) (1999) 121–132.
[13] M.F. Modest, Radiative Heat Transfer, second ed., Academic Press, New York, 2003.
[14] A.J. Chandy, D.J. Glaze, S.H. Frankel, A hybrid large eddy simulation/filtered mass density function for calculation of strongly radiating turbulent flames, J. Heat Transfer 131 (5) (2009) 51201.
[15] D. Veynante, L. Vervisch, Turbulent combustion modeling, Prog. Energy Combust. Sci. 28 (3) (2002) 193–266.
[16] C.K. Law, Comprehensive description of chemistry in combustion modeling, Combust. Sci. Technol. 177 (5) (2005) 845–870.
[17] M. Frenklach, Reaction mechanism of soot formation in flames, Phys. Chem. Chem. Phys. 4 (2002) 2028–2037.
[18] Z. Qin, V.V. Lissianski, H. Yang, W.C. Gardiner, S.G. Davis, H. Wang, Combustion chemistry of propane: a case study of detailed reaction mechanism optimization, Proc. Combust. Inst. 28 (2000) 1663–1669.
[19] R.J. Kee, G. Dixon-Lewis, J. Warnatz, M.E. Coltrin, J.A. Miller, A computer code package for evaluation of gas-phase, multicomponent transport properties, Tech. Rep. SAND86-8246, Sandia National Laboratories, 1986.
[20] R.J. Kee, F.M. Rupley, J.A. Miller, CHEMKIN-II: a Fortran chemical kinetics package for the analysis of gas-phase chemical kinetics, Tech. Rep. SAND89-8009B, Sandia National Laboratories, 1989.
[21] Y.Z. Zhang, D.C. Haworth, A general mass consistency algorithm for hybrid particle/finite-volume PDF methods, J. Comp. Phys. 194 (1) (2004) 156–193.
[22] H. Bockhorn, Soot Formation in Combustion, Springer-Verlag, New York, 1994.
[23] P. Lindstedt, Simplified soot nucleation and surface growth steps for non-premixed flames, in: H. Bockhorn (Ed.), Soot Formation in Combustion: Mechanisms and Models, Springer-Verlag, New York, 1994.
[24] H. Wang, D.X. Du, C.J. Sung, C.K. Law, Experiments and numerical simulation on soot formation in opposed-jet ethylene diffusion flames, Proc. Combust. Inst. 26 (1996) 2359–2368.
[25] K.G. Neoh, J.B. Howard, A.F. Sarofim, in: S.D.C.G. Smith (Ed.), Particulate Carbon: Formation During Combustion, Plenum, New York, 1981, p. 261.
[26] I.M. Kennedy, Models of soot formation and oxidation, Progr. Energy Combust. Sci. 23 (2) (1997) 95–132.
[27] M. Frenklach, H. Wang, Detailed modeling of soot particle nucleation and growth, Proc. Combust. Inst. 23 (1991) 1559–1566.
[28] S.J. Harris, A.M. Weiner, Chemical kinetics of soot particle growth, Annu. Rev. Phys. Chem 36 (1985) 31–52.
[29] M. Frenklach, Mehod of moments with interpolative closure, Chem. Eng. Sci. 57 (12) (2002) 2229–2239.
[30] C. McEnally, A. Schaffer, M. Long, L. Pfefferle, M. Smooke, M. Colket, R. Hall, Computational and experimental study of soot formation in a coflow, laminar ethylene diffusion flame, Proc. Combust. Inst. 27 (1998) 1497–1505.
[31] A. Kazakov, M. Frenklach, Dynamic modeling of soot particle coagulation and aggregation: implementation with the method of moments and application to high-pressure laminar premixed flames, Combust. Flame 114 (3–4) (1998) 484–501.
[32] M.B. Colket, R.J. Hall, Successes and uncertainties in modeling soot formation in laminar, premixed flames, in: H. Bockhorn (Ed.), Soot Formation in Combustion: Mechanisms and Models, Springer-Verlag, New York, 1994.
[33] D.C. Haworth, Progr. Energy Combust. Sci. (2009).
[34] S.B. Pope, PDF methods for turbulent reactive flows, Progr. Energy Combust. Sci. 11 (2) (1985) 119–192.
[35] S. Subramaniam, S.B. Pope, A mixing model for turbulent reactive flows based on euclidean minimum spanning trees, Combust. Flame 115 (4) (1998) 487–514.
[36] A.R. Masri, S. Subramaniam, S.B. Pope, A mixing model to improve the PDF simulation of turbulent diffusion flames, Proc. Combust. Inst. 26 (1996) 49–57.
[37] S.B. Pope, Particle method for turbulent flows: integration of stochastic model equations, J. Comp. Phys. 117 (2) (1995) 332–349.
[38] M. Muradoglu, P. Jenny, S.B. Pope, D.A. Caughey, A consistent hybrid finite volume/particle method for the PDF equations of turbulent reactive flows, J. Comp. Phys. 154 (2) (1999) 342–371.
[39] P. Jenny, S.B. Pope, M. Muradoglu, D.A. Caughey, A hybrid algorithm for the joint PDF equation of turbulent reactive flows, J. Comp. Phys. 166 (2) (2001) 218–252.
[40] S.V. Subramaniam, D.C. Haworth, A PDF method for turbulent mixing and combustion on three-dimensional unstructured deforming meshes, Int. J. Eng. Res. 1 (2) (2000) 171–190.
[41] L. Wang, M.F. Modest, D.C. Haworth, S.R. Turns, Modeling nongray soot and gas-phase radiation in luminous turbulent nonpremixed jet flames, Combust. Theory Model. 9 (3) (2005) 479–498.
[42] L. Wang, D.C. Haworth, S.R. Turns, M.F. Modest, Interactions among soot, thermal radiation, and NO_x emissions in oxygen-enriched turbulent nonpremixed flames: a CFD modeling study, Combust. Flame 141 (1–2), 170–179.

[43] S. Mazumder, M.F. Modest, A PDF approach to modeling turbulence–radiation interactions in nonluminous flames, Int. J. Heat Mass Transfer 42 (1999) 971–991.
[44] G. Li, M.F. Modest, Application of composition PDF methods in the investigation of turbulence–radiation interactions, J. Quant. Spectrosc. Radiat. Transfer 73 (2–5) (2002) 461–472.
[45] P.J. Coelho, O.J. Teerling, D. Roekaerts, Spectral radiative effects and turbulence/radiation interaction in a non-luminous turbulent jet diffusion flame, Combust. Flame 133 (1–2) (2003) 75–91.
[46] L. Tessé, F. Dupoirieux, J. Taine, Monte Carlo modeling of radiative transfer in a turbulent sooty flame, Int. J. Heat Mass Transfer 47 (2004) 555–572.
[47] A.Y. Snegirev, Statistical modeling of thermal radiation transfer in buoyant turbulent diffusion flames, Combust. Flame 136 (1–2) (2004) 51–71.
[48] A. Wang, M.F. Modest, Monte Carlo simulation of radiative heat transfer and turbulence interactions in methane/air jet flames, J. Quant. Spectrosc. Radiat. Transfer 109 (2007) 269–279.
[49] G. Li, Investigation of turbulence–radiation interactions by a hybrid FV/PDF Monte Carlo method, Ph.D. Thesis, The Pennsylvania State University, University Park, PA, 2002.
[50] A. Wang, M.F. Modest, Photon Monte Carlo simulation for radiative transfer in gaseous media represented by discrete particle fields, J. Heat Transfer 128 (10) (2006) 1041–1049.
[51] P.J. Coelho, Numerical simulation of the interaction between turbulence and radiation in reactive flows, Progr. Energy Combust. Sci. 33 (4) (2007) 311–383.
[52] A. Wang, M.F. Modest, Spectral Monte Carlo models for nongray radiation analyses in inhomogeneous participating media, Int. J. Heat Mass Transfer 50 (19–20) (2007) 3877–3889.
[53] A. Wang, Investigation of turbulence–radiation interactions in turbulent flames using a hybrid finite volume/Monte Carlo approach, Ph.D. Thesis, The Pennsylvania State University, 2007.
[54] M.F. Modest, H. Zhang, The full-spectrum correlated-k distribution for thermal radiation from molecular gas–particulate mixtures, J. Heat Transfer 124 (1) (2002) 30–38.
[55] H. Chang, T.T. Charalampopoulos, Determination of the wavelength dependence of refractive indices of flame soot, Proc. R. Soc. London, A 430 (1880) (1990) 577–591.
[56] R.S. Mehta, M.F. Modest, D.C. Haworth, Radiation characteristics and turbulence–radiation interactions in sooting turbulent jet flames, Combust. Theory Model. (2009), submitted for publication.
[57] S.B. Pope, Turbulent Flows, Cambridge University Press, Cambridge, 2000.
[58] V. Saxena, S.B. Pope, PDF simulations of turbulent combustion incorporating detailed chemistry, Combust. Flame 117 (1–2) (1999) 340–350.
[59] R.S. Mehta, Detailed modeling of soot formation and turbulence–radiation interactions in turbulent jet flames, Ph.D. Thesis, The Pennsylvania State University, 2008.
[60] A. Coppalle, D. Joyeux, Temperature and soot volume fraction in turbulent diffusion flames: measurements of mean and fluctuating values, Combust. Flame 96 (3) (1994) 275–285.
[61] J.H. Kent, D. Honnery, Soot and mixture fraction in turbulent diffusion flames, Combust. Sci. Technol. 54 (1) (1987) 383–398.
[62] N.E. Endrud, Soot, radiation and pollutant emissions in oxygen-enhanced turbulent jet flames, Master's thesis, The Pennsylvania State University, University Park, PA, 2000.
[63] M. Kalal, K.A. Nugent, Abel inversion using fast Fourier transforms, Appl. Opt. 27 (10) (1988) 1956–1959.
[64] L. Wang, N.E. Endrud, S.R. Turns, M.D. D'Agostini, A.G. Slavejkov, A study of the influence of oxygen index on soot, radiation, and emission characteristics of turbulent jet flames, Combust. Sci. Technol. 178 (8) (2002) 45–72.
[65] R.V. Bandaru, Experimental studies of the emission characteristics of nonpremixed gas–air flames of various configurations, Ph.D. Thesis, The Pennsylvania State University, University Park, PA, 2000.
[66] L. Wang, Detailed chemistry, soot, and radiation calculations in turbulent reacting flows, Ph.D. Thesis, The Pennsylvania State University, 2005.
[67] A. Wang, M.F. Modest, High-accuracy, compact database of narrow-band k-distributions for water vapor and carbon dioxide, J. Quant. Spectrosc. Radiat. Transfer 93 (2005) 245–261.